Origin of the Giant Spin-Detection Efficiency in Tunnel-Barrier-Based Electrical Spin Detectors

E. Fourneau,[1,*] A.V. Silhanek[2] and N.D. Nguyen[1]

[1]*Solid-State Physics—Interfaces and Nanostructures, Q-MAT, CESAM, University of Liège, Liège 4000, Belgium*
[2]*Experimental Physics of Nanostructured Materials, Q-MAT, CESAM, University of Liège, Liège 4000, Belgium*

Efficient conversion of a spin signal into an electric voltage in mainstream semiconductors is one of the grand challenges of spintronics. This process is commonly achieved via a ferromagnetic tunnel barrier, where nonlinear electric transport occurs. In this work, we demonstrate that nonlinearity may lead to a spin-to-charge conversion efficiency larger than 10 times the spin polarization of the tunnel barrier when the latter is under a bias of a few millivolts. We identify the underlying mechanisms responsible for this remarkably efficient spin detection as the tunnel-barrier deformation and the conduction-band shift resulting from a change of applied voltage. In addition, we derive an approximate analytical expression for the detector spin sensitivity $P_{\text{det}}(V)$. Calculations performed for different barrier shapes show that this enhancement is present in oxide barriers as well as in Schottky-tunnel barriers, even if the dominant mechanisms differ with the barrier type. Moreover, although the spin signal is reduced at high temperatures, it remains superior to the value predicted by the linear model. Our findings shed light onto the interpretation and understanding of electrical spin-detection experiments and open paths to optimizing the performance of spin-transport devices.

I. INTRODUCTION

The injection, transport, and detection of a spin-polarized current in a nonmagnetic (NM) semiconductor (SC) are cornerstones of spintronics. In recent years, encouraging results have been obtained on spin-polarized current injection into mainstream group-IV semiconductors such as Si [1–3] and Ge [4–6] at room temperature, as well as into other promising materials such as graphene [7,8]. To that purpose, ferromagnetic (FM) tunnel junctions are widely regarded as one of the best approaches to both generating a spin polarization in a SC and converting it into a voltage signal. This is in part due to the limited spin absorption in the FM and the reduced resistance mismatch [9]. Nowadays, the literature is abundant with works quantifying the performance of a FM tunnel barrier to generate and detect a spin signal in a SC as well as in evaluation of the spin lifetime [10]. Promising results have been reported over the past decade with a surprising and unexpected spin-detection efficiency, demonstrating in some cases a pickup voltage higher than the injected spin signal [4,11–13]. This outstanding spin detection has been reported for devices where the FM tunnel contact used for detection has been biased, as in technologically relevant devices

[14–18]. This amplification effect offers an interesting perspective for on-chip integration of spin-based circuits and has attracted considerable attention from the theoretical standpoint. Indeed, various tentative mechanisms have been proposed over recent years to explain the observed large spin-detection efficiency, such as two-step tunneling [19,20], thermionic emission [21], or lateral-current inhomogeneity [22], to name just a few. Unfortunately, none of the above-mentioned mechanisms seems to satisfactorily account for all the experimental findings.

Recently, it has been experimentally established that some discrepancies between experiments and theoretical calculations find their origin in the energy dependence of the carrier transmission probability in the tunnel junction [12,13,23–28]. This suggests that a description based on nonlinear transport of spin should be invoked [29]. Although preliminary ideas in this direction have already been advanced some 10 years ago, it is not until recently that nonlinearities have been recognized as an essential ingredient for the understanding of FM tunnel junctions. In this work, we aim at identifying the implications of nonlinearity in FM tunnel junctions using a theoretical approach, including crucial aspects overlooked in previous studies while being directly responsible for the giant spin-detection efficiency. This approach allows us to explain how a spin signal can be converted into a charge signal with an efficiency of several hundreds of percent. It is

---

*emile.fourneau@uliege.be

worth noting that the obtained results apply to any spin-detection device composed of a FM/SC contact where direct tunneling transport occurs and therefore relevant not only to oxide and tunnel barriers but also to various pseudosubstrates such as graphene and other two-dimensional (2D) materials.

II. LINEAR MODEL OF SPIN DETECTION

The measurement of a voltage variation due to the presence of a spin polarization is called electrical spin detection. This mechanism is achieved by the transfer of carriers through a spin-dependent barrier (B) formed at the interface between a FM layer and a NM layer. In this section, we briefly introduce the model based on a linear-transport description through a tunnel barrier sandwiched between a FM and a NM metal [9,10]. The model assumes that the conductance of the barrier depends on the spin orientation. We denote by G_+ and G_- the conductance, respectively, for spin parallel and antiparallel to the main magnetization of the FM contact. The application of a voltage bias $V_{app} \equiv -\mu_v/e$, μ_v being the NM electrochemical potential and e the elementary charge, will force the transfer of charge carriers from one side of the interface to the other side with a spin preference. In this model, it is assumed that a preferential spin population has been generated in the NM via an external mechanism (e.g., spin carriers are electrically injected from another FM contact or via optical generation), leading to a splitting of the electrochemical potential $\mu_s = \mu_+ - \mu_-$ at the B/NM interface [see Fig. 1(a)]. It is also considered that the spin

accumulation under the detector is homogeneous (i.e., the detector width is much smaller than the diffusion length). In presence of spin accumulation, the spin-dependent current density through the barrier, i.e., from the NM into the FM, is given by

$$J_\pm = \frac{G_\pm}{A}\left(\frac{\mu_v}{e} \pm \frac{\mu_s}{2e}\right), \tag{1}$$

where A is the junction cross-section area. The total current is

$$J = J_+ + J_- = \frac{G}{Ae}\left(\mu_v + P_G\frac{\mu_s}{2}\right), \tag{2}$$

where $G = G_+ + G_-$ the total conductance barrier and $P_G = (G_+ - G_-)/G$ is the spin polarization of the tunnel conductance. The tunnel-junction bias is

$$V_{app} = -\frac{\mu_v}{e} = -\frac{JA}{G} + P_G\frac{\mu_s}{2e}. \tag{3}$$

The last term of Eq. (3) represents a voltage signal due to the spin accumulation and is called the spin voltage $V_{spin} = -P_G\mu_s/(2e)$. The figure of merit of a device designed for spin detection, namely the spin-detection efficiency, is defined as the electrical voltage generated at the detector per unit of spin accumulation, $P_{det} = -V_{spin}/(\mu_s/2e)$, which equals P_G in the linear model.

Since the linear model for spin transport is based on Ohm's law, the tunnel barrier is therefore considered as a conductance G independent of any applied voltage. This
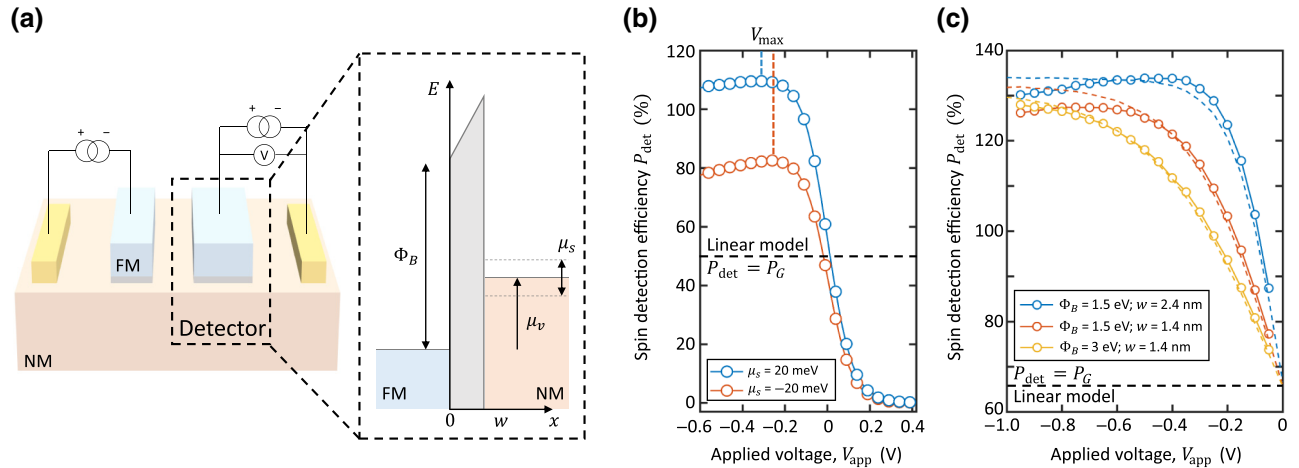

FIG. 1. The nonlinear spin-detection efficiency under bias. (a) A schematic energy-band diagram of the FM/B/NM tunnel contact under a voltage bias, where $\mu_v = -eV_{app}$ is the applied electrochemical potential and w and Φ_B are the width and the height of the barrier. A drawing of the entire spintronic device is also provided for clarity. (b) The computed spin-detection efficiency with tunnel bias for two different spin accumulations μ_s ($w = 4$ nm; $\Phi_B = 1$ eV; $P_G = 50\%$; $T = 1$ K). The dashed line is obtained by canceling the barrier deformation under bias, corresponding to the linear model. (c) The spin-detection efficiency as a function of the applied voltage for different barrier dimensions. The dashed lines correspond to results reported in Ref. [29].

consideration is unrealistic, as the tunneling process is strongly nonlinear and is the essence of the spin-filtering effect.

III. NONLINEAR MODEL

Although the linear theory for spin injection and detection captures the essential mechanisms of these processes, deviations from the linear model have been systematically reported in experiments based on three-terminal (3T) Hanle devices and in four-terminal (4T) devices where both the injector and the detector are under bias [10,16]. Recently, Jansen et al. [29] experimentally observed that the spin-detection efficiency P_{det} at a tunnel junction strongly depends on the applied bias, offering a way to magnify the detected spin accumulation. In their work, the authors pointed out that the spin signal amplification is inherent to the nonlinear transport occurring at the tunnel junction, which arises from the dependence of the transmission probability on the energy of the injected carriers. In simple words, since the transmission probability increases with the energy, the preferential spin population will undergo a higher impact than the minority spin population when changing the applied voltage. Naturally, the increase of P_{det} with the applied voltage could be attributed mainly to this effect.

While this reasoning seems to qualitatively capture the trend observed in most experimental results, there still exist some features that remain unexplained [29]. Notably, in these authors' explication of the origin of the nonlinearity, the fact that the increase in the applied voltage needs to compensate the loss of current after spin precession (i.e., the spin voltage) becomes sensitive to the increase of the junction bias, leading to a P_{det} that is *independent* of the bias. Moreover, their model looks limited, as it may not be able to justify why a signal differing by several order of magnitude is pointed out in many spin tunnel devices [10]. In this work, we aim at investigating the mechanisms governing this nonlinear transport by using an incremental approach, which in complexity is progressively added to the model. We focus first on the simplest model of a tunnel barrier between two metals (FM/B/NM), where the effects of the barrier deformation under bias and the importance of the spin-accumulation intensity are thoughtfully investigated. Then, the NM metal is replaced by a highly degenerate SC in order to evaluate the impact of a band gap, the degeneracy level, and the energy dependence of the density of states (DOS). At a later stage, we address the variation of the tunnel-barrier shape to compare the detection efficiency of oxide and Schottky-tunnel barriers.

Calculations are performed by solving the spin-dependent nonlinear tunnel-transport equations based on the two-channel model, as described in Refs. [9,30]. The problem is presumed to be stationary in order to match the experimental measuring conditions of usual spin-detection

experiments. In this work, a spin-dependent description of the tunnel current density is used for a semiclassical approach [31–33]:

$$J_{\pm} = \frac{e}{h} \frac{1 \pm P_G}{2} \times \int_{-\infty}^{\infty} T(E, V_{app}) \left[n_{2D}(E, \mu_v \mp \mu_s/2) - n_{2D,fm}(E, 0) \right] dE, \quad (4)$$

where h is Planck's constant, e is the elementary charge, and E is the longitudinal component of the carrier energy (i.e., perpendicular to the barrier). Using the WKB approximation, the transmission function is given by [34]

$$T(E, V_{app}) = \exp\left(-\frac{4m^\star e}{h^2} \int_{x_L}^{x_R} \sqrt{\phi(x, V_{app}) - E} \, dx \right), \quad (5)$$

where $m^\star$ is the electron effective mass, $\phi(x, V_{app})$ is the barrier profile, and x is the space coordinate perpendicular to the barrier plane [Fig. 1(a)], with x_L and x_R as the left and right turning points of the barrier (where $\phi = E$). The WKB method presents certain limitations regarding the range of energy for the particle and the barrier-profile steepness, as it assumes that the wave number varies slowly with the position [31]. This hypothesis is satisfied for a large trapezoidal barrier (i.e., when $w\sqrt{\phi_{mean}} \gg 0.4 \, \text{nm} \, \text{eV}^{1/2}$) [35]. For barriers with a geometry such that a narrowing of the barrier width takes place at a higher potential, as for a Schottky-tunnel barrier, it has been shown that the WKB approximation can predict the tunnel current with appreciable accuracy if the barrier lowering is neglected [36,37].

In Eq. (4), n_{2D} is the 2D electron density and is given by

$$n_{2D}(E, \mu) = \frac{4m^\star k_B T \pi}{h^2} \ln\left[1 + \exp\left(\frac{\mu - E}{k_B T} \right) \right], \quad (6)$$

where k_B is Boltzman's constant and T is the absolute temperature. It is assumed that the spin dependence of the carrier transport has two origins. First, the density of carriers with spin up and down in the NM layer will differ even if the DOS is spin independent. This effect is due to the presence of a spin accumulation and is expressed in the 2D electron density. Second, the spin conductance of the barrier P_G varies with the applied voltage, as it depends on the tunnel transmission function and the FM DOS, which varies strongly from one material to another. A possibility for including the energy-dependent DOS into the calculation is to consider a parabolic DOS with a shift of energy between spin up and down, giving a spin conductance P_G that decreases with the applied bias [38]. In this work, we intentionally ignore this variation in order to highlight the effect of tunnel barrier on the detected signal. Further discussion on the combined effects of the

tunnel barrier and the energy-dependent FM DOS on the spin-detection efficiency can be found in the Supplemental Material [39]. The spin voltage is obtained by comparing the total current under a given bias V_{app} in the presence of a spin accumulation μ_s in the NM layer, with the total current corresponding to a compensated bias $V_{app} + V_{comp}$ in the absence of spin accumulation. The spin voltage V_{spin} equals the voltage V_{comp} for which both total currents are identical:

$$J\left(V_{app}, \mu_s\right) = J\left(V_{app} + V_{comp}, 0\right). \tag{7}$$

Indeed, in a typical spin-detection experiment, the applied voltage is compensated with a voltage V_{spin} to maintain a constant current through the junction irrespective of the level of spin accumulation.

A. Origin of the nonlinear dependence $P_{det}(V_{app})$

We first investigate the case of a rectangular tunnel barrier (B) in a three-layer FM/B/NM stack [Fig. 1(a)]. Although this model has already been studied previously [29], in the present work the FM quasi-Fermi level is set as the reference electrode and the oxide-barrier deformation with applied voltage is considered. As for the linear model, we consider that the spin accumulation is homogeneous and is generated via an external mechanism. We also assume that the intensity of the spin accumulation is not perturbed by the change of the voltage bias. Indeed, the spin accumulation generated by the detector current as well as the impact of a drift effect in the channel can be excluded by adopting an adequate experimental protocol [40,41].As illustrated in Fig. 1(b), the spin-detection efficiency P_{det} strongly depends on the junction bias. At 0 V, the spin detection bears the value that is predicted by the linear model. However, when the structure is under a nonzero external bias, P_{det} strongly deviates from the linear model, increasing or decreasing in magnitude for negative bias (spin-extraction regime) and positive bias (spin-injection regime), respectively. While the general behavior of P_{det} as a function of V_{app} is similar to the results of Jansen *et al.* [29], our findings provide further unanticipated features. First, the nonlinear effect does not show a perfect odd symmetry and $P_{det}(V)$ exhibits a nonmonotonic dependence (not due to a change of P_G), leading to a maximal detection efficiency for a specific voltage V_{max}. Second, the maximal value of P_{det} is not limited to $2P_G$. Moreover, the value depends on the tunnel-barrier dimensions, as is demonstrated below. Finally, P_{det} is very sensitive to the intensity of the spin accumulation in the vicinity of the barrier. Concerning the origin of this nonlinearity, it has previously been suggested that the general behavior of P_{det} as a function of V_{app} for both the injection and the extraction regimes may be related to the steepness of the energy dependence of the barrier transmission function $dT(E)/dE$ [29]. Indeed, the spin accumulation mainly

affects the transport of electrons of higher energy. As the bias decreases ($V_{app} < 0$), high-energy electrons make an increasingly dominant contribution to the device current as a consequence of the exponential energy dependence of $T(E)$, thus leading to a higher impact of the spin accumulation on the carrier transport. On the other hand, for positive biases, the spin accumulation impacts the tail of the transmission function, resulting in a weaker perturbation of the transport through the barrier. Consequently, the more prominent the slope of $T(E)$, the more important is the nonlinearity of the spin detection.

B. Effect of the barrier deformation

Although the steepness of the transmission function is correlated with the nonlinear behavior of $P_{det}(V_{app})$, it is not directly responsible for the change in the spin-detection efficiency. In this section, we demonstrate that the enhancement of P_{det} is actually determined by the deformation of the barrier when the device is under an applied bias. As shown in Fig. 2(a), a variation of the bias leads to a deformation of the barrier, producing a significant change in the transmission function. For negative
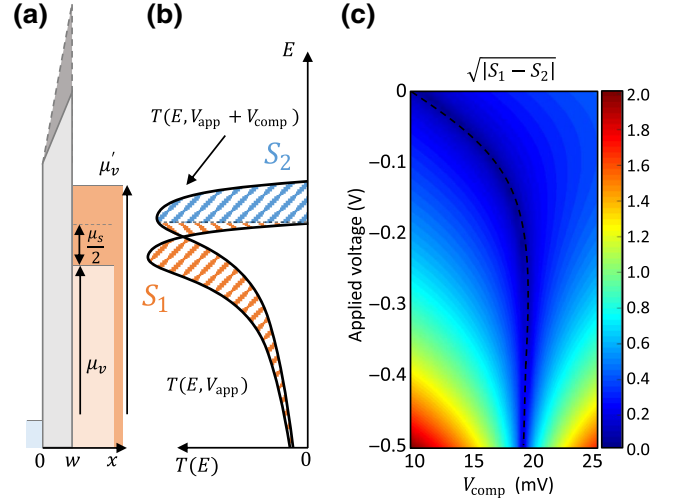

FIG. 2. (a) A schematic representation of the barrier deformation for two different values of the applied voltage associated with $\mu_v = -eV_{app}$ (light color) and $\mu'_v = -eV_{app} - eV_{comp}$ (dark color). (b) Sketches of the corresponding transmission functions under these conditions: the hatched areas correspond to the two contributions to the current variation due to the bias change. S_1 is integrated from $-\infty$ to $\mu_v + \mu_s/2$ and represents the change of current due to the reduction of the barrier permeability compensated by the increased number of available carriers with a longitudinal energy lower than $\mu_v + \mu_s/2$. In the linear regime of spin detection, $S_1 = 0$. S_2 is integrated from $\mu_v + \mu_s/2$ to μ'_v and corresponds to the gain of current resulting from the enhancement of V_{spin} in comparison with the linear model. (c) The variation of $\sqrt{|S_1 - S_2|}$ with the spin voltage and the applied bias. Along the dashed line, the two areas are equal and $V_{comp} = V_{spin}$.

biases, the barrier height mean value increases when V_{app} becomes more negative. In the same way, the voltage compensation V_{comp} also triggers a reduction of transmission through the barrier, therefore resulting in a positive reinforcement of this potential compensation and then a higher P_{det}. In Fig. 2(b), we show a sketch of the energy dependence of the transmission function through a barrier under two different biases; respectively, $\mu_v = -eV_{app}$ in the presence of spin accumulation μ_s and $\mu_v' = -eV_{app} - eV_{comp}$ in the absence of spin accumulation. For the sake of simplicity, we consider a barrier spin polarization of $P_G = 100\%$ (the effect of the barrier spin polarization at zero bias is discussed later). Moreover, without loss of generality, calculations are done for a positive spin accumulation. As presented in Fig. 1(b), the general behavior of $P_{det}(V)$ remains unchanged and the rationale proposed hereafter to explain the enhancement of P_{det} is valid irrespective of the value of μ_s: the tunnel current in a spin-detection experiment is proportional to the integrated transmission $T(E)$ from $E = -\infty$ to the value of the electrochemical potential associated with the applied bias, at low temperature. By integrating from $-\infty$, we assume that the potential energy of the metal is far below its Fermi level, which is an acceptable approximation as the contribution of the low-energy carriers decreases exponentially [31]. The areas resulting from the integration, which determine the spin-detection efficiency, are highlighted in Fig. 2(b). The area S_1 corresponds to the effect of electrons with a longitudinal energy of less than $\mu_v + \mu_s/2$. This area represents the decrease of the tunnel current resulting from the reshaping of the barrier, partially compensated by a gain due to the increase of available carriers (with a total energy between $\mu_v + \mu_s/2$ and $\mu_v + \mu_{comp}$). The area S_2 corresponds to the gain of current due to the increase of the bias (from $|\mu_s/(2e)|$ up to V_{comp}). As a voltage compensation of $|\mu_s/(2e)|$ corresponds to the prediction of the linear model, S_2 directly reflects the nonlinearity. As demonstrated in the Supplemental Material [39], S_1 and S_2 may be approximated as follows:

$$S_1 \simeq \int_0^{\mu_v + \mu_s/2} \left[-V_{comp} \frac{df(E, V_{app})}{dV} (\mu_v + \mu_{comp} - E) \right.$$
$$\left. - \left(\mu_{comp} - \frac{\mu_s}{2} \right) \right] T(E, V_{app}) dE, \tag{8}$$

$$S_2 \approx \frac{1}{2} \left(\mu_{comp} - \frac{\mu_s}{2} \right)^2 T(\mu_v, V_{app}), \tag{9}$$

where $f(E, V_{app})$ is directly related to the transmission function defined in Eq. (5) through $T(E, V_{app}) = \exp \left[f(E, V_{app}) \right]$. As mentioned above, the area S_1 is composed of two terms. The first one is positive (for negative bias) and corresponds to the barrier deformation. The second one is negative when $\mu_{comp} > \mu_s/2$ and reflects the

gain of carriers with a high total energy. The increase in voltage V_{comp} needed to obtain a perfect compensation of S_1 by S_2 is the spin voltage $V_{spin} = (\mu_v - \mu_v')/(-e)$, which is measured in a spin-detection experiment. As soon as $S_2 > 0$, the response becomes nonlinear and the spin voltage becomes larger than $P_G \mu_s/2$.

In Fig. 2(c), we show the difference $|S_1 - S_2|$ for a specific range of bias and voltage compensation values. The dashed line denotes the combinations for which both integrals are equals. This line reproduces the behavior of the spin-detection efficiency as a function of the junction voltage, as shown in Figs. 1(b) and 1(c), with a sharp rise followed by a slow decay of the spin-detection efficiency as the voltage increases in absolute value. As a key consequence, we realize that the relative evolutions of S_1 and S_2 ultimately determine P_{det} through a link between the bias and the energy dependencies of the tunnel-barrier transmission. In Figs. 3(a) and 3(b), we plot the evolution of both areas, as a function of V_{app} and V_{comp}, respectively, offering a graphical resolution of the spin-detection experiment. Such a plot represents a powerful tool to track the value of quantities such as S_1 and S_2, which are essential to understanding the electrical spin-detection mechanism in the presence of nonlinear transport.

In what follows, we focus exclusively on negative values of the applied voltage, since for this voltage polarity an increase of the spin-detection efficiency is expected. First, we observe in Fig. 3(a) that, for large polarizations, both integrals are exponential functions of V_{app}, with a similar exponential decay, while S_1 deviates abruptly from
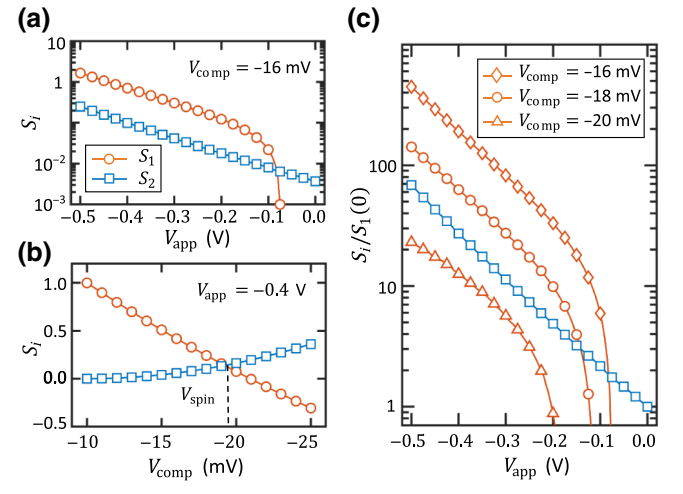

FIG. 3. The competition between the gain and loss of tunnel current in a spin-detection experiment bearing nonlinear transport. The evolution of integration areas S_i (index i refers to 1 or 2) with (a) the applied bias (semilogarithmic scale) and (b) the compensation voltage (linear scale). (c) The relative shift of S_2 (blue) in comparison to S_1 (orange) for different spin voltages (semilogarithmic scale).

this decay for weak polarizations, until it becomes negative. In Fig. 3(b), it is shown that both areas increase with the compensation voltage when the applied voltage is kept constant. Based on these equations and on Fig. 3(b), we observe that $S_2(V_{comp})$ shows a parabolic evolution, with a slope determined by the transmission probability of a particle with energy $E = \mu_v = -eV_{app}$, while the area S_1 is less sensitive to a change of compensation voltage. Therefore, as shown in Fig. 3(c), a variation of the compensation voltage ultimately translates into an offset for S_1 relative to S_2. In the voltage range in which S_1 is rapidly varying with V_{app}, an increase of V_{comp} will decrease S_1 with respect to S_2, combined with a slight increase of the bias voltage, for which the intersection $S_1 = S_2$ occurs. On the other hand, for larger bias, a change in V_{comp} will produce a strong increase of the bias at the intersection $S_1 = S_2$, due to the fact that S_1 and S_2 have nearly the same exponential decay. If we refer to Eqs. (8) and (9), a similar slope in logarithmic scale is possible only if the transmission function $T(E, V)$ is large enough to dominate the integral in the definition of S_1. Such is the case if the upper integration limit is large enough. Considering the previous explanation, the large increase in the spin-detection efficiency under a low applied voltage, and the slow decrease at a higher bias, are related to the deviation of S_1 from S_2, [i.e., deviation from the exponential nature of $T(E, V)$].The foregoing argumentation allows us to explain the physical origin of the existence of an optimal value V_{max} for the spin-detection efficiency, as indicated in Fig. 1(b). On the one hand, the range of electron energies that participate in the current increases with the bias (from 0 to μ_v, if we assimilate the Fermi-Dirac distribution to a steplike function, as is the case for sufficiently low temperatures). The current gain caused by an increase of the spin voltage is then due to electrons of the higher energy levels. On the other hand, the reduction of barrier permeability impacts the transmission probability of all energy levels. When the range of energy levels concerned is narrow enough (V_{app} weak), the transmission function varies slowly with the energy and, subsequently, the participation of low-energy electrons is not negligible. Therefore, a higher spin voltage is needed to compensate for the current loss due to the reduction of the tunneling capacity of the electrons for all energy levels. However, as the transmission through the barrier evolves exponentially with the energy, the current due to electrons with energies lower than the NM quasi-Fermi level [μ_v in Fig. 2(a)] becomes less significant. In addition, this reduction of transmission is progressively compensated by the increase of carriers with high total energy. For a certain negative bias, the current gain resulting from the spin-voltage compensation overcomes the loss due to the barrier deformation, leading to a decrease of P_{det}. The competition between the two effects leads to a maximum spin-detection efficiency at a bias V_{max}. This result is in agreement with recent experimental observations [29], suggesting that the
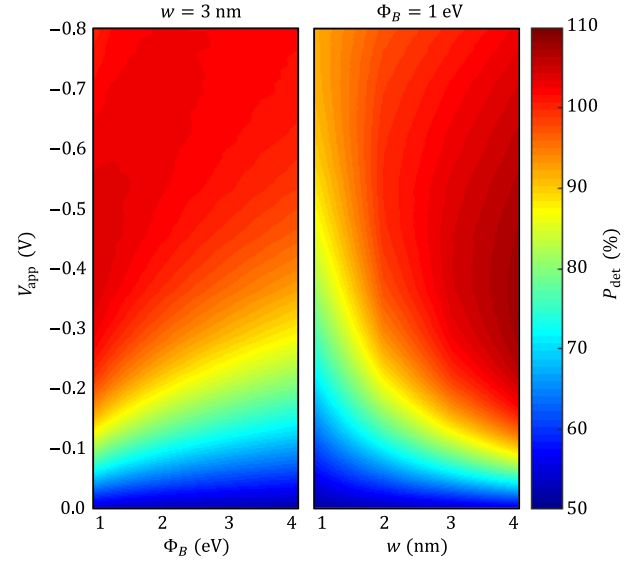

FIG. 4. The effect of the variation of the rectangular-barrier dimensions on the spin-detection efficiency. The results are obtained for $P_G = 50\%$ and $\mu_s = 10$ meV.

present description may shed light on how to optimize the spin-detection efficiency by tuning the barrier parameters.

Indeed, the energy dependence of the transmission function as well as the way it varies under bias are essential ingredients that are needed to understand and master the spin-detection efficiency. As explained previously, P_{det} is sensitive to the barrier properties (width and height) as well as the spin polarity. Figure 4 summarizes the dependence of P_{det} on the barrier dimensions. It can be observed that the variation of the width w and of the height Φ_B have opposing impacts on P_{det}. For weak negative biases, the variation of P_{det} with V_{app} is larger for lower and thicker barriers, i.e., for a sharper transmission-function $T(E)$ slope. It is worth noting that the maximum spin-detection efficiency $P_{det}(V_{max})$ also increases for thinner and taller barriers, although the corresponding variations are less significant. This increase is related to a stronger barrier deformation as df/dV increases with w and decreases with Φ_B [39]. On the other hand, as the exponential growth of the transmission probability gets higher, the voltage at which the high-energy electrons dominate the spin-detection efficiency is reached at a lower value $|V_{max}|$.

C. Effect of the degeneracy level

The experimental observations in Ref. [29] demonstrate that the spin-detection efficiency in a rectangular barrier may overcome the theoretical limit of $2P_G$ to reach a spin detection of 2.3 times the value predicted by the linear model and even more when taking the drastic reduction of P_G with bias into account. As the barrier used in that experimental work is rectangular (2-nm-thick MgO [1]), the increase in the spin-detection efficiency cannot be

explained solely by barrier deformation with the applied bias. Indeed, based on our calculations, the spin-detection efficiency is expected to be lower than twice the barrier spin polarization P_G. However, as shown in the following discussion, the observed excess spin detection can be justified by including the effect of the band gap in the model. This mechanism is presented below for a FM/B/SC structure, where SC is a nonmagnetic degenerate semiconductor. In order to describe the semiconductor with its band gap, we introduce the parameter ϵ, which reflects the degree of degeneracy of the semiconductor. ϵ represents the difference between the electrochemical μ_v potential and the edge of the conduction band. This effect is included in our calculation by introducing an energy-dependent DOS $N(E)$ in the NM layer, given by

$$N(E) = \frac{8\pi\sqrt{2}}{h^3} m^{3/2} \sqrt{E - (\mu_v - \epsilon)}. \qquad (10)$$

The DOS is therefore null for energies in the band gap, i.e., for $E < \mu_v - \epsilon$. At low temperatures, μ_v corresponds to the maximal occupied energy level in this band. Therefore, the parameter ϵ is linked to the carrier concentration in the conduction band by the Fermi-Dirac distribution. Figure 5(a) sketches the basic case of a FM/B/SC sandwich structure, including the band gap. The consequence of the band gap on the transport of electrons
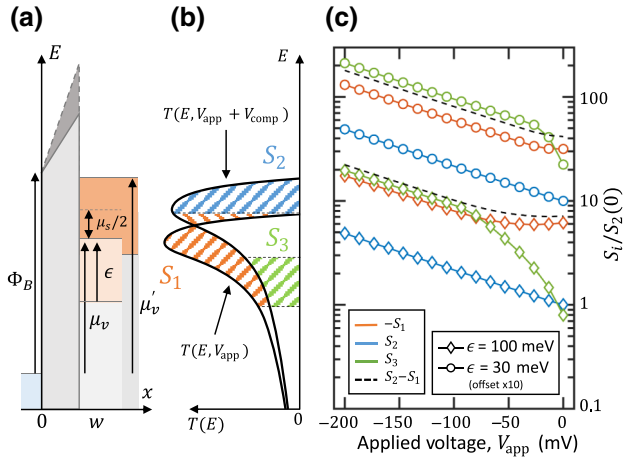

(a)   (b)   (c)

FIG. 5. The effect of the SC band gap on the spin-detection efficiency. (a) A schematic representation of a FM/B/SC structure for a degenerated SC. The Fermi level is located at an energy value of ϵ above the bottom of the conduction band E_c. The barrier and the E_c edge change as the bias is set to μ'_v (without spin accumulation $\mu_s = 0$—dark color) instead of μ_v (with spin accumulation—light color). (b) A qualitative sketch of the corresponding transmission function. The S_3 integral is associated with the current loss due to the energy shift of the band gap. (c) A quantitative analysis of the variation of the areas S_1, S_2, and S_3 with the applied junction voltage for $V_{\text{comp}} = -20$ mV, $\mu_s = 10$ meV and for two different values of ϵ. The areas (for each value of ϵ) are normalized by $S_1(0)$ and are offset.

through the barrier is visible when the applied electrochemical potential μ_v overcomes the degeneracy level ϵ. In this case, electrons that tunnel from the SC into the FM have energies limited by the bottom of the conduction band and not by the occupancy in the FM. As a consequence, when a compensation voltage is applied after removing the spin accumulation, the increase of potential from μ_v to μ'_v is accompanied by an increase of the energy level of the bottom of the conduction band. In terms of the current integration area, it corresponds to a third area S_3 that corresponds to a loss of current due to the shift of E_c induced by a change of applied voltage [see Fig. 5(b)]. It is approximated as

$$S_3 \approx \mu_{\text{comp}} \left(\frac{\mu_{\text{comp}}}{2} + \epsilon \right) T(\mu_v, V_{\text{app}}). \qquad (11)$$

As demonstrated in the Supplemental Material [39], in addition to the area S_3, the insertion of the band gap will modify the definition of S_1:

$$
\begin{aligned}
S_1 &\simeq \left(\frac{\mu_s}{2} + \epsilon \right) \left(\alpha + \beta \frac{df}{dV} + \gamma \frac{df}{dE} \right) T(\mu_v, V_{\text{app}}), \\
\alpha &= \left(\frac{\mu_s}{2} - \mu_{\text{comp}} \right), \\
\beta &= -V_{\text{comp}} \left(\mu_{\text{comp}} - \frac{\mu_s}{4} + \frac{\epsilon}{2} \right), \\
\gamma &= \alpha \left(\frac{\mu_s}{2} - \epsilon \right).
\end{aligned}
\qquad (12)
$$

As μ_{comp} is positive and larger than $\mu_s/2$ (for negative bias at the detector), α is strictly negative. This reflects the gain of tunnel current due to the increase of charge carriers. The second term, $\beta > 0$, is linked to the reduction of the transmission through the barrier and increases with ϵ. The last term, γ, is also positive because $\mu_s/2 < \epsilon$, as the density of spins, is limited to the density of carriers. Both S_1 and S_3 contribute to the reduction of the tunnel current and their respective contributions are dependent on the level of degeneracy. As ϵ decreases, S_1 will decrease and S_3 will increase. For weak values of ϵ, $|\alpha| \gg |\beta(df/dV) + \gamma(df/dE)|$ and S_1 becomes negative.

$$S_1 \simeq \left(\frac{\mu_s}{2} + \epsilon \right) \left(\frac{\mu_s}{2} - \mu_{\text{comp}} \right) T(\mu_v, V_{\text{app}}). \qquad (13)$$

As shown in Fig. 5(c), at high applied voltages, all areas follow a similar exponential decay, determined by $T(\mu_v, V_{\text{app}})$. For lower biases ($\mu_v < \epsilon$), the effect of the band-gap shift is limited by the absence of empty states in the FM under the Fermi level; therefore the impact of S_3 on the spin-detection efficiency is reduced for highly doped SC (ϵ large). In contrast to that, for a SC with a weaker level of degeneracy, the shift of the band gap will reduce the tunnel current proportionally to the compensation voltage. As a consequence, a spin-detection efficiency

higher than twice the barrier polarity is possible. Under the approximation $\mu_v \gg \epsilon > \mu_s/2$, we propose an analytical model to predict the nonlinearity of the spin-detection efficiency at low temperature. In this case, as demonstrated in the Supplemental Material [39],

$$P_{\text{det}} \approx \frac{\frac{\mu_s}{2}\left(1 + \frac{\epsilon}{2}\frac{df}{dE}\right) + P_G\left[2\epsilon + \frac{1}{2}\left(\left(\frac{\mu_s}{2}\right)^2 - \epsilon^2\right)\frac{df}{dE}\right]}{\epsilon^2\left(\frac{df}{dE} - \frac{1}{e}\frac{df}{dV}\right)},$$

(14)

where the derivatives of $f(E, V)$ are evaluated for $E = \mu_v$ and $V = V_{\text{app}}$. The dependence with respect to the barrier shape and deformation is determined by the partial derivatives of the function $f(E, V)$. As predicted in our simulations, $P_{\text{det}} \sim \epsilon^{-1}$. As an indication, in the case of an n-type silicon substrate, a doping level between 5×10^{18} and 1×10^{20} cm^{-3} corresponds to a value of ϵ between 0.01 and 0.1 eV. In Fig. 6, the effect of a variation of the barrier height and width is analyzed. The presence of the band gap severely modifies the spin-detection response due to the barrier deformation under bias (see Fig. 4), since P_{det} now decreases with an increase of the width and a decrease of the barrier height. We conclude that the impact of S_3 is less important for barriers with a steeper transmission-energy dependence. Indeed, for a barrier with a sharp transmission probability, the current due to electrons with a weak energy (range of energy for S_3) is negligible in comparison to those of higher energy (range of S_2). Therefore, a reduction of the energy dependence of the transmission probability acts as an increase of the degeneracy level. The

results from Fig. 6 show that P_{det} reaches huge values—of several thousands of percent—while P_G is only 50%. Such a large nonlinearity factor may explain the reported deviation of several orders of magnitude between the (linear) theory and the Hanle experiments achieved in 3T devices [10]. While we focus here exclusively on degenerate semiconductors, we note that the presence of a depletion region at the B/SC interface can influence the detected spin signal due to an additional Schottky barrier, with a depletion width depending on the degeneracy level ϵ. For highly doped SC, this barrier is rather thin and, therefore, carriers can tunnel through both tunnel barriers [42], resulting in one larger barrier with a nonrectangular shape. Our calculations predict that the intensity of spin injection may be enhanced if two-step tunneling via interfacial states occurs. However, this effect is important only for a highly resistive depletion region (which is not the case in our model) [20]. Concerning the spin-detection efficiency, a more critical point is to define how the effective barrier height of the depletion layer is changing with the potential (i.e., this change corresponds to the voltage drop at the oxide barrier, which is different from the applied voltage) [43]. Our calculations show that only the latter can impact the spin-detection efficiency strongly, while P_{det} is only weakly affected by the change of depletion width with the doping level. A more in-depth discussion of this point is presented in the Supplemental Material [39], whereas in the next section we focus on the effect of the barrier shape. It is important to stress that our analysis is only dedicated to degenerate SC. For devices with nondegenerate SC, in which thermionic emission dominates the transport in the
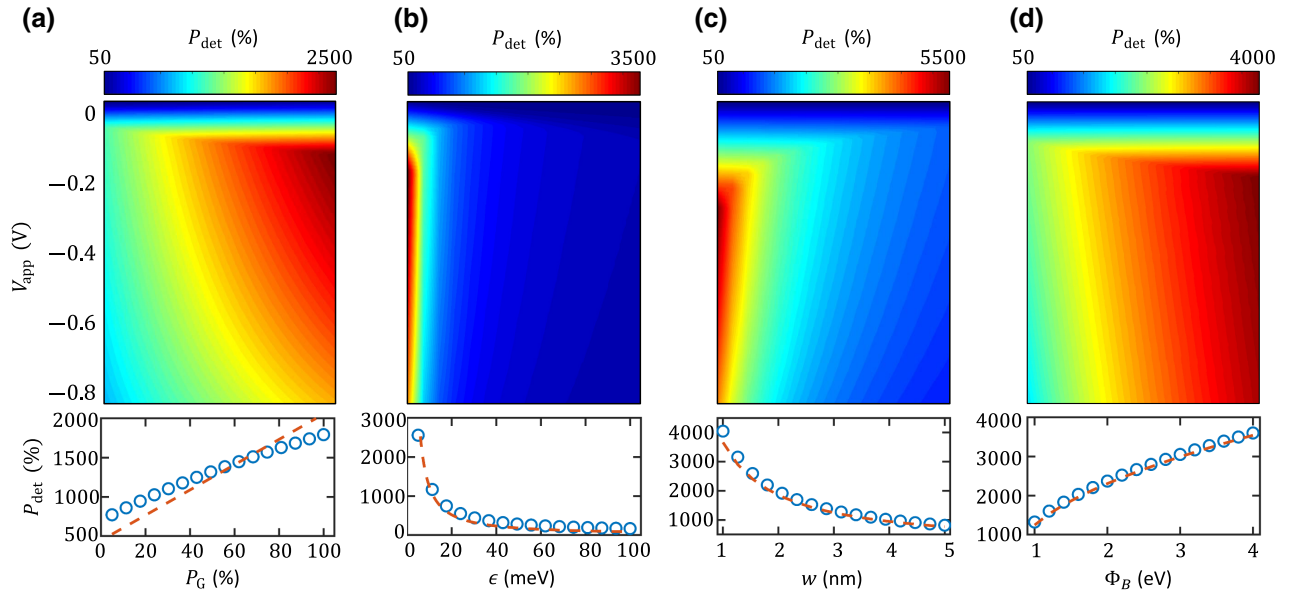

FIG. 6. The effect of the variation of the rectangular-barrier parameters—(a) P_G, (b) ϵ, (c) w, and (d) Φ_B—on the spin-detection efficiency when the band gap affects the tunnel transport. The fixed parameters are $P_G = 50\%$, $\epsilon = 10$ meV, $w = 3$ nm, and $\Phi_B = 1$ eV. The bottom panels compare results of simulations with the analytical solution from Eq. (14) for $V_{\text{app}} = -0.8$ V.

depletion region, it has been shown that the depletion layer drastically affects the detected spin voltage even if spin signals much higher than that predicted by the linear model are calculated [44]. To complete the analysis, the intermediate case of moderately doped SC should be investigated, as unexpected huge spin-voltage values have been experimentally probed in a device in which thermally assisted tunneling occurs [4].

D. Effect of barrier shape

In a tunnel barrier designed for electrical spin detection, if a negative bias is applied, both the deformation of the barrier transmission and the change of energy range for carriers that participate to the transport are responsible for the observation of a colossal nonlinear spin-detection efficiency. For rectangular barriers, the second phenomenon seems to dominate, except for highly degenerate SC. The numerical simulations as well as the analytical approach indicate that the nonlinearity of the spin detection is sensitive to the steepness of the energy dependence of the transmission function. Steeper transmission may be obtained if a nonrectangular tunnel barrier is used.

At low bias, the behavior of S_1 is directly dependent on the barrier shape [39]. In this section, we quantify the degree of sensitivity of S_1 to that critical feature of the interface. The comparison is made for four different shapes, a rectangular, triangular, parabolic, and exponential spatial dependence, respectively [see Fig. 7(a)]. Each barrier is determined by a maximal height Φ_B, a width w, and a level of degeneracy ϵ. The way in which those parameters influence the shape of the barrier is detailed in the Supplemental Material [39]. The width associated with

each barrier (2, 3, 3, and 3 nm, respectively) is arbitrarily chosen in order to have a transmission probability in the same range of values. The maximal barrier height at zero current is set to $\Phi_B = 1$ eV.

The transmission function of each barrier (at $V_{\text{app}} = 0$) is plotted in Fig. 7(b). As expected, the steepness of the transmission function for electrons with an energy close to the quasi-Fermi level increases from the rectangular barrier to the exponential one.

Spin-detection efficiencies under different biases are computed for a constant spin accumulation of $\mu_s = 10$ meV. The results are presented for the FM/B/NM and FM/B/SC structures [Figs. 7(c) and 7(d)]. This allows us to separate the effect of the barrier-shape modification from that of the band gap. Indeed, except for the case of the rectangular barrier, a change of ϵ does lead to a reshaping of the barrier. For the model that does not include the band gap, P_{det} tends to the value of $2P_G$ for a rectangular tunnel barrier, while the maximal spin-detection efficiency skyrockets when the barrier height depends on the distance from the FM/B interface. This huge variation of the detected spin signal is explained by two major factors. First, because of their energy-dependent width, nonrectangular barriers have a higher change of transmission probability induced by the voltage compensation [39]. Second, as the transmission increases more abruptly with the particle energy, the reduction of available carriers with high longitudinal energy has less impact on the total current (i.e., the negative part of area S_1 is reduced in Fig. 2). The higher variation of the transmission probability with the energy is also responsible for the decrease in the detection efficiency with applied bias, at higher negative voltage. Additional electrons due to the compensation voltage have
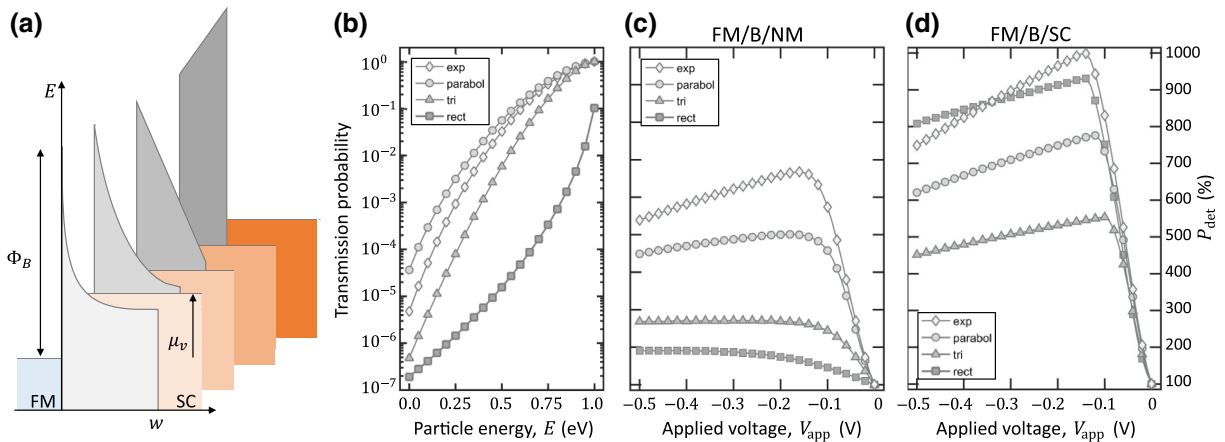

FIG. 7. (a) A schematic representation of the different shapes of the interface barrier, from the background to the front: rectangular, triangular, parabolic, and exponential evolution of the barrier height with the distance from the SC. (b) The energy dependence of the transmission probability through the barrier. (c),(d) The nonlinearity of the spin-detection efficiency with the applied voltage for tunnel barriers with various shapes. The results depicted in (c) show the effect of the barrier shape for a FM/B/NM configuration, while those shown in (d) focus on the FM/B/SC case. The calculations are performed using $w = 3$ nm (except for the rectangular barrier, where $w = 2$ nm), $\Phi_B = 1$ eV, $P_G = 100\%$, $T = 1$ K, and $\epsilon = 50$ meV.

a higher tunnel probability and therefore compensate the spin accumulation more easily.

For the case of a barrier sandwiched between a FM metal and a degenerate SC, the maximal spin-detection efficiency is improved irrespective of the barrier shape. However, the rectangular barrier is more sensitive to a change of ϵ, since it is correlated with the steepness of the transmission function, as explained in Sec. III C. It is worth noting that a change of ϵ does modify the spin transport through two different mechanisms. First, it reduces the range of carrier energies involved in the tunnel transport. Second, it changes the shape of the barrier, as could be expected for a Schottky junction. We conclude that the huge spin-detection efficiency improvement due to the nonlinearity of the tunnel junction arises in every type of barrier, as previously suggested by Jansen et al. [29]. However, in contrast to the latter study, we demonstrate that the dominant mechanism varies between an oxide-based tunnel junction and a FM/SC contact Schottky junction, which is a nuance that we deem important for understanding the whole picture.

E. Dependence on μ_s and spin lifetime

In addition to the correction of the amplitude of the predicted spin accumulation that is formed in the SC, calculations performed in our study suggest that the predicted spin lifetime in Hanle-precession experiments needs to be adjusted. Such a correction arises from the fact that the applied voltage affects the spin-detection efficiency and therefore the spin accumulation μ_s will also induce a deviation of P_{det} from P_G. In the nonlinear theory, a higher spin voltage is linked to a higher barrier deformation which, in turn, triggers an increase of the spin voltage. Therefore, the spin voltage is expected to deviate from a linear dependence with the spin accumulation. As shown in Fig. 8(a), our results highlight this observation and it is shown that P_{det} is proportional to μ_s [45]. This result obviously impacts the spin diffusion length deduced in Hanle-precession measurements. The theory underlying such processes implies that the spin accumulation is destroyed when applying a magnetic field perpendicular to the spin preferential orientation of magnetization [46]. Under a magnetic field B, the spin accumulation $\mu_s(B)$ follows a Lorentzian shape, with a maximum value $\mu_s(0)$. From the full width at half maximum (FWHM) of the Lorentzian function, one can deduce the spin lifetime of carriers injected into the NM layer, namely $\tau_{sf} = 2/(\text{FWHM})$. However, this kind of experiment is performed on the spin voltage instead of the spin accumulation.

Therefore, in the nonlinear-transport regime, a modified Lorentzian distribution is needed. Supposing that $P_{\text{det}} = \alpha\mu_s + \beta$ for an applied voltage V_{app}, the variation of V_{spin}
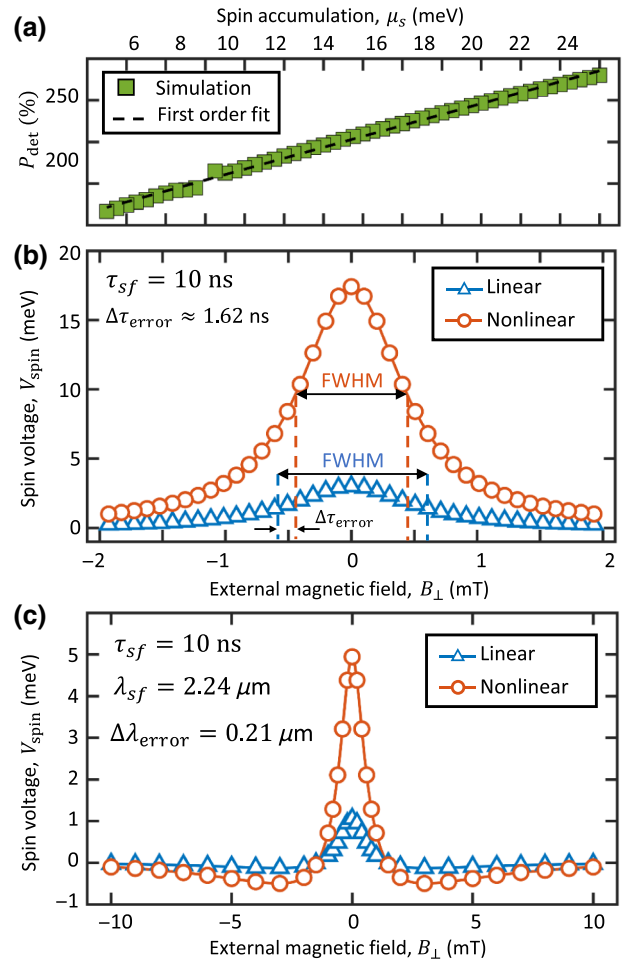
FIG. 8. The consequences of the variation of the spin-detection efficiency with the spin accumulation. (a) The computed value of P_{det} for different spin accumulations in the vicinity of a tunnel rectangular barrier ($w = 3$ nm, $\Phi_B = 1$ eV, $P_G = 30\%$, $V_{\text{app}} = -800$ mV, $\epsilon = 50$ meV). (b),(c) numerical simulation of a 3T spin-precession experiment (b) and a 4T spin-diffusion experiment (c). In (b), the spin voltage is plotted (based on the linear model and considering the nonlinear effect) with the corresponding spin lifetime, assuming that both curves are Lorentzian distributions. In (c), the spin-diffusion length is extracted by fitting with the analytical solution of the one-dimensional (1D) spin-diffusion model.

with the magnetic field becomes

$$V_{\text{spin}}(\omega_L) = \frac{\mu_s(0)}{2\left[1 + (\omega_L \tau_{sf})^2\right]}\left[\frac{\alpha\mu_s(0)}{1 + (\omega_L \tau_{sf})^2} + \beta\right],$$
(15)

where ω_L is the Landau frequency, which is linearly dependent on the magnetic field B. Consequently, we suggest a correction for the equation that allows one to extract the spin lifetime from Hanle-precession measurements,

$$\tau_{sf} = \frac{2}{FWHM}\sqrt{\frac{\sqrt{\beta^2 + 2\alpha\mu_s(0)(\alpha\mu_s(0)+\beta)} - \alpha\mu_s(0)}{\alpha\mu_s(0)+\beta}}. \quad (16)$$

According to Eq. (14), the ratio between α and β can be simplified to give the following approximation:

$$\frac{\alpha\mu_s(0)}{\beta} = \frac{\mu_s}{4P_G\epsilon}. \quad (17)$$

As a consequence, the error on the spin lifetime is expected to be negligible for a device with a highly degenerate semiconductor. However, for spin accumulation in the range of the degeneracy level, the correction factor may reach a dozen percent, as shown in Fig. 8(b). This figure shows the bell-shape variation of the spin voltage with the perpendicular magnetic field intensity. The spin accumulation is assumed to be 20 meV at zero magnetic field, leading to a detected spin voltage of 3 mV (with $P_G = 30\%$) according to the linear model. The result is compared to the curve obtained for similar $\mu_s(B)$ but including the features of nonlinear transport. While both curves can be accurately fitted using a Lorentzian curve, the extracted value of the spin accumulation and the spin lifetime are not correct due to the nonlinearity. An error of 10% for τ_{sf} is probed and the value of μ_s is overestimated by a factor of 5 if the effects of nonlinearity are neglected. As these errors are strongly sensitive to the spin-tunnel-barrier properties as well as to the intensity of the spin accumulation, we evaluate the error for a large panel of barrier properties (the results are detailed in the Supplemental Material [39]). Typically, for a degeneracy level of 10 meV and a spin accumulation of 4 meV, one obtains an error between 0 and 60%, depending on the value of P_G. While this effect may appear significant, it depends greatly on the ratio between the spin accumulation at zero magnetic field and the level of degeneracy. The estimation of errors on the spin lifetime based on results currently reported in the literature is minor, as the ratio between the detected spin accumulation and the level of degeneracy is low. Indeed, in 3T devices, the detected spin voltage generally ranges from tens to hundreds of microvolts, while the degeneracy levels are of the order of 10 meV and thus the errors are systematically lower than 5% for devices based on oxide tunnel barriers [12,29,47,48]. However, recent advances in fabrication processes lead progressively to an increase of the detected signal by decreasing parasitic effects such as interface roughness [49]. For instance, Spiesser *et al.* have achieved spin detection (without bias-detector enhancement) of dozens of millivolts [1]. In addition, it is worth noting that the error is expected to grow rapidly with the applied current, as $\mu_s(0)$ increases while P_G decreases and ϵ remains fixed.

While having a nonzero voltage is inevitable in the 3T design, the detector is typically free from bias in the nonlocal spin device. However, as the application of a bias to the detector could be used to improve the signal-to-noise ratio in the spin-precession measurement, it is relevant to evaluate the error for the extraction of the diffusion length. In Fig. 8(c), we compare the probed spin signal in the linear condition (no bias voltage to the detector) with the nonlinear case. The calculations are achieved by solving the 1D Bloch equation with an added diffusion term that describes spin diffusion in the presence of the spin-orbit coupling and an external magnetic field [50]. The spin diffusion coefficient and spin lifetime are material properties fixed at $D_{\mathrm{spin}} = 5\ \mathrm{cm}^2/\mathrm{s}$ and $\tau_{sf} = 10$ ns, respectively. The spin diffusion length is extracted by fitting the spin signal with a solution of the modified Bloch equation. For reasons identical to those presented for the 3T design, the comparison leads to an error close to 10%, which is corrected if the fitting equation is adapted to include the linear dependence between P_{det} and μ_s. It is worth noting that the error due to the nonlinearity is directly related to the intensity of the spin accumulation. Indeed, the higher the ratio $\alpha\mu_s/\beta$, the higher is the error if a linear model is used.

F. Effect of the temperature

In order to complete our analysis of the nonlinearity of the spin-detection efficiency under bias, we perform simulations for different temperatures. In Fig. 9(a), $P_{\mathrm{det}}(V_{\mathrm{app}})$ is plotted for a range of temperatures from 1 K to 300 K and shows that the spin detection is less efficient at high temperatures. This behavior has been systematically observed in 3T devices, in which the reduction of the spin voltage with temperature has been attributed to an increase of the thermal noise, an increase of the thermionic emission transport, and a simultaneous reduction of the spin polarity of the barrier P_G [1]. As those effects are not included in the present calculations, the decrease of the detected spin signal with temperature should be ascribed to another phenomenon. More precisely, the temperature dependence of the detection efficiency can be simply linked to the broadening of the Fermi-Dirac function. As the temperature increases, the Fermi-Dirac distribution deviates from the steplike Heaviside function. As a result, carriers with energies slightly higher than the quasi-Fermi level will participate in the charge transport through the tunnel barrier. Consequently, carriers with a higher transmission probability will be involved. Therefore, the gain of current due to the increase of the applied voltage V_{comp} will be
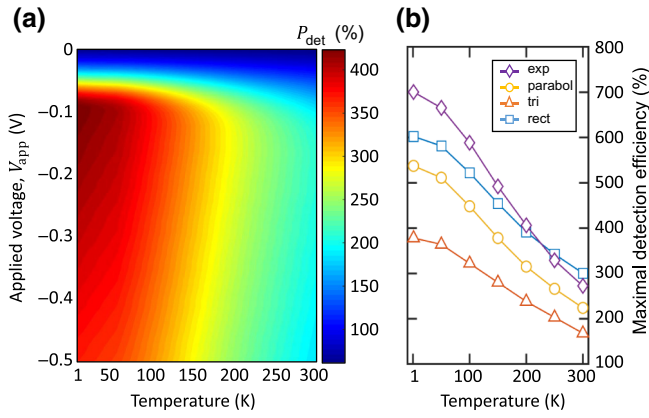
(a)

(b)

FIG. 9. The effect of temperature on the spin-detection efficiency. (a) The variation of P_{det} with the temperature and the junction bias. (b) A comparison of the temperature effect on different barrier shapes. The calculations are performed using barrier properties as presented in Fig. 7. (a) $\epsilon = 50$ meV, $P_G = 50\%$, $\Phi_B = 1$ eV, and $w = 3$ nm. (b) The same, except for the rectangular case: $w = 2$ nm.

increased. This effect may be seen as an increase of the carrier concentration in the conduction band (i.e., an increase of ϵ), which results in a reduction of the spin-detection efficiency. The results depicted in Fig. 9(b) show the effect of temperature for the different barrier shapes that are studied in this work. It is noted that the maximal spin-detection efficiency decreases for all barrier shapes. At low temperature, the effect is more pronounced for the nonrectangular barrier, suggesting that its origin is related to the steepness of the energy dependence of the transmission function. This outcome tends to confirm the justification that higher temperatures allow the activation of carriers with higher energies (associated with higher barrier transmission) and, therefore, that the current is compensated more easily by the increase of the compensation voltage. For barriers with sharp transmission functions, the gain of current due to high-energy carriers will obviously be higher.

IV. CONCLUSION

In summary, we demonstrate that the nonlinearity of the spin-detection efficiency under bias results from two different mechanisms: the tunnel-barrier deformation and the conduction-band shift, leading to a spin-detection efficiency higher than 10 times that predicted by the linear model. As a consequence, we emphasize the need to take into account the effect of the energy dependence of the tunneling transmission probability as well as the band gap (even for highly degenerate SC) in the model used to analyze results from local (2T and 3T) spin devices. The effects of the doping level, the barrier shape, and the temperature on the magnitude of the probed spin voltage and spin relaxation time are studied, leading to

a better interpretation of the spin-detection experiments. We believe that our results clarify the complex mechanisms that govern spin injection, transport, and detection experiments and help to explain numerous puzzling results reported in the literature.

[1] A. Spiesser, H. Saito, Y. Fujita, S. Yamada, K. Hamaya, S. Yuasa, and R. Jansen, Giant Spin Accumulation in Silicon Nonlocal Spin-Transport Devices, Phys. Rev. Appl. **8,** 064023 (2017).
[2] T. Suzuki, T. Sasaki, T. Oikawa, M. Shiraishi, Y. Suzuki, and K. Noguchi, Room-temperature electron spin transport in a highly doped Si channel, Appl. Phys. Express **4,** 023003 (2011).
[3] M. Ishikawa, T. Oka, Y. Fujita, H. Sugiyama, Y. Saito, and K. Hamaya, Spin relaxation through lateral spin transport in heavily doped n-type silicon, Phys. Rev. B **95,** 115302 (2017).
[4] A. Spiesser, H. Saito, R. Jansen, S. Yuasa, and K. Ando, Large spin accumulation voltages in epitaxial Mn5Ge3 contacts on Ge without an oxide tunnel barrier, Phys. Rev. B **90,** 205213 (2014).
[5] M. Yamada, M. Tsukahara, Y. Fujita, T. Naito, S. Yamada, K. Sawano, and K. Hamaya, Room-temperature spin transport in n-Ge probed by four-terminal nonlocal measurements, Appl. Phys. Express **10,** 093001 (2017).
[6] Y. Fujita, M. Yamada, M. Tsukahara, T. Oka, S. Yamada, T. Kanashima, K. Sawano, and K. Hamaya, Spin Transport and Relaxation up to 250 K in Heavily Doped n-Type Ge Detected Using Co2FeAl0.5Si0.5 Electrodes, Phys. Rev. Appl. **8,** 014007 (2017).
[7] M. Ohishi, M. Shiraishi, R. Nouchi, T. Nozaki, T. Shinjo, and Y. Suzuki, Spin injection into a graphene thin film at room temperature, Jpn. J. Appl. Phys. **46,** L605 (2007).
[8] N. Tombros, C. Jozsa, M. Popinciuc, H. T. Jonkman, and B. J. V. Wees, Electronic spin transport and spin precession in single graphene layers at room temperature, Nature **448,** 571 (2007).
[9] A. Fert and H. Jaffrès, Conditions for efficient spin injection from a ferromagnetic metal into a semiconductor, Phys. Rev. B **64,** 184420 (2001).
[10] R. Jansen, S. P. Dash, S. Sharma, and B. C. Min, Silicon spintronics with ferromagnetic tunnel devices, Semicond. Sci. Technol. **27,** 083001 (2012).
[11] X. Lou, C. Adelmann, M. Furis, S. A. Crooker, C. J. Palmstrøm, and P. A. Crowell, Electrical Detection of Spin Accumulation at a Ferromagnet-Semiconductor Interface, Phys. Rev. Lett. **96,** 176603 (2006).
[12] M. Ishikawa, H. Sugiyama, T. Inokuchi, K. Hamaya, and Y. Saito, Effect of the interface resistance of CoFe/MgO contacts on spin accumulation in silicon, Appl. Phys. Lett. **100,** 252404 (2012).

[13] T. Sasaki, T. Suzuki, Y. Ando, H. Koike, T. Oikawa, Y. Suzuki, and M. Shiraishi, Local magnetoresistance in Fe/MgO/Si lateral spin valve at room temperature, Appl. Phys. Lett. **104**, 052404 (2014).

[14] S. Datta and B. Das, Electronic analog of the electro-optic modulator, Appl. Phys. Lett. **56**, 665 (1990).

[15] S. Datta, How we proposed the spin transistor, Nat. Electron. **1**, 604 (2018).

[16] Y. Fujita, M. Yamada, M. Tsukahara, T. Naito, S. Yamada, K. Sawano, and K. Hamaya, Nonmonotonic bias dependence of local spin accumulation signals in ferromagnet/semiconductor lateral spin-valve devices, Phys. Rev. B **100**, 024431 (2019).

[17] A. Spiesser, Y. Fujita, H. Saito, S. Yamada, K. Hamaya, S. Yuasa, and R. Jansen, Hanle spin precession in a two-terminal lateral spin valve, Appl. Phys. Lett. **14**, 242401 (2019).

[18] T. Naito, M. Yamada, S. Yamada, and T. Kanashima, Inverse local magnetoresistance effect up to room temperature in ferromagnet-semiconductor lateral spin-valve devices, Mat. Sci. Semicon. Proc. **113**, 105046 (2020).

[19] M. Tran, H. Jaffrès, C. Deranlot, J. George, A. Fert, A. Miard, and A. Lemaître, Enhancement of the Spin Accumulation at the Interface between a Spin-Polarized Tunnel Junction and a Semiconductor, Phys. Rev. Lett. **102**, 036601 (2009).

[20] R. Jansen, A. M. Deac, H. Saito, and S. Yuasa, Injection and detection of spin in a semiconductor by tunneling via interface states, Phys. Rev. B **134420**, 134420 (2012).

[21] R. Jansen, A. Spiesser, H. Saito, and S. Yuasa, Nonlinear spin transport in a rectifying ferromagnet/semiconductor Schottky contact, Phys. Rev. B **92**, 075304 (2015).

[22] S. P. Dash, S. Sharma, R. S. Patel, M. P. de Jong, and R. Jansen, Electrical creation of spin polarization in silicon at room temperature, Nature **462**, 491 (2009).

[23] M. Kameno, Y. Ando, E. Shikoh, T. Shinjo, T. Sasaki, T. Oikawa, T. Suzuki, Y. Suzuki, and M. Shiraishi, Effect of spin drift on spin accumulation voltages in highly doped silicon, Appl. Phys. Lett. **101**, 122413 (2012).

[24] M. Ishikawa, H. Sugiyama, T. Inokuchi, K. Hamaya, and Y. Saito, Spin transport and accumulation in n^+-Si using Heusler compound Co_2FeSi/MgO tunnel contacts, Appl. Phys. Lett. **107**, 092402 (2016).

[25] T. A. Peterson, S. J. Patel, C. C. Geppert, K. D. Christie, A. Rath, D. Pennachio, and M. E. Flatt, Spin injection and detection up to room temperature in Heusler alloy/n-GaAs spin valves, Phys. Rev. B **93**, 235309 (2016).

[26] T. Tahara, Y. Ando, M. Kameno, H. Koike, K. Tanaka, S. Miwa, Y. Suzuki, T. Sasaki, T. Oikawa, and M. Shiraishi, Observation of large spin accumulation voltages in nondegenerate Si spin devices due to spin drift effect: Experiments and theory, Phys. Rev. B **93**, 214406 (2016).

[27] M. Oltscher, F. Eberle, T. Kuczmik, A. Bayer, D. Schuh, D. Bougeard, M. Ciorga, and D. Weiss, Gate-tunable large magnetoresistance in an all-semiconductor spin-transistor-like device, Nat. Commun. **8**, 1807 (2017).

[28] S. Sato, R. Nakane, T. Hada, and M. Tanaka, Spin injection into silicon in three-terminal vertical and four-terminal lateral devices with Fe/Mg/MgO/Si tunnel junctions having

an ultrathin Mg insertion layer, Phys. Rev. B **96**, 235204 (2017).

[29] R. Jansen, A. Spiesser, H. Saito, Y. Fujita, S. Yamada, K. Hamaya, and S. Yuasa, Nonlinear Electrical Spin Conversion in a Biased Ferromagnetic Tunnel Contact, Phys. Rev. Appl. **10**, 064050 (2018).

[30] P. C. Van Son, H. Van Kempen, and P. Wyder, Boundary Resistance of the Ferromagnetic-Nonferromagnetic Metal Interface, Phys. Rev. Lett. **58**, 2271 (1987).

[31] J. H. Davies, *The Physics of Low-Dimensional Semiconductors: An Introduction* (Cambridge University Press, New-York, 1997).

[32] E. L. Wolf, *Principles of Electron Tunneling Spectroscopy* (Oxford University Press, New York, 1989).

[33] R. Tsu and L. Esaki, Tunneling in a finite superlattice, Appl. Phys. Lett. **22**, 562 (1973).

[34] M. Razeghi, *Fundamentals of Solid State Engineering* (Springer Publishing Company, Incorporated, Evanston, 2009), 3rd ed., Chap. 4.

[35] K. Gundlach and J. Simmons, Range of validity of the WKB tunnel probability, and comparison of experimental data and theory, Thin Solid Films **4**, 61 (1969).

[36] R. A. Vega, Comparison study of tunneling models for Schottky field effect transistors and the effect of Schottky barrier lowering, IEEE Trans. Electron. Devices **53**, 1593 (2006).

[37] S. Kale and P. N. Kondekar, Design and investigation of dielectric engineered dopant segregated Schottky barrier MOSFET with NiSi source/drain, IEEE Trans. Electron. Devices **64**, 4400 (2017).

[38] S. O. Valenzuela, D. J. Monsma, C. M. Marcus, V. Narayanamurti, and M. Tinkham, Spin Polarized Tunneling at Finite Bias, Phys. Rev. Lett. **94**, 196601 (2005).

[39] See the Supplemental Material at http://link.aps.org/supplemental/10.1103/PhysRevApplied.14.024020 for a complete development of the analytical approaches to the integration surfaces, the nonlinear prediction of the spin voltage, and details about the different barrier shapes.

[40] M. Gurram, S. Omar, and B. J. V. Wees, Bias induced up to 100% spin-injection and detection polarizations in ferromagnet/bilayer-hBN/graphene/hBN heterostructures, Nat. Commun. **8**, 248 (2017).

[41] To ensure that the enhancement of the spin signal is only due to an increase of the spin-detection efficiency and not due to drift effect, a two-step measurement is suggested. For each injector bias voltage V_{inj}, the spin signal is detected for a 0 V bias at the detector, $V_{det} = 0$ V and for $V_{det} = V_{inj}$ (this equality holds only if the two electrodes have the same area). This approach allows us to avoid the spin-drift effect in the channel as well as the change of spin accumulation with the injection current level.

[42] R. Jansen, B. Min, S. Dash, S. Sharma, G. Kioseoglou, A. Hanbicki, O. van 't Erve, P. Thompson, and B. Jonker, Electrical spin injection into moderately doped silicon enabled by tailored interfaces, Phys. Rev. B **82**, 241305(R) (2010).

[43] A. Türüt, B. Bati, A. Kökce, M. Saglam, and N. Yalcin, The bias-dependence change of barrier height of Schottky diodes under forward bias by including the series resistance effect, Phys. Scr. **53**, 118 (1996).

[44] R. Jansen and B. C. Min, Detection of a Spin Accumulation in Nondegenerate Semiconductors, Phys. Rev. Lett. **99,** 246604 (2007).

[45] The deviation of $P_{\mathrm{det}}(\mu_s)$ from the linear fit for μ_s close to 0 is due to the definition of P_{det} as the ratio between the spin voltage and half of the spin accumulation, leading to numerical uncerntainty. However, our analytical solution shows that the linear approximation for $P_{\mathrm{det}}(\mu_s)$ is improved if μ_s and ϵ are small. Moreover, it is worth noting that P_{det} has no physical meaning for the case of zero spin accumulation.

[46] I. Žutić, J. Fabian, and S. D. Sarma, Spintronics: Fundamentals and applications, Rev. Mod. Phys. **76,** 323 (2004).

[47] M. Kameno, Y. Ando, E. Shikoh, T. Shinjo, T. Sasaki, T. Oikawa, Y. Suzuki, T. Suzuki, and M. Shiraishi, Effect of spin drift on spin accumulation voltages in highly doped silicon, Appl. Phys. Lett. **104,** 092409 (2014).

[48] A. T. Hanbicki, S. Cheng, R. Goswami, O. M. J. V. Erve, and B. T. Jonker, Electrical injection and detection of spin accumulation in Ge at room temperature, Solid State Commun. **152,** 244 (2012).

[49] S. P. Dash, S. Sharma, J. C. Le Breton, J. Peiro, H. Jaffrès, J. M. George, A. Lemaître, and R. Jansen, Spin precession and inverted Hanle effect in a semiconductor near a finite-roughness ferromagnetic interface, Phys. Rev. B **84,** 054410 (2011).

[50] M. Johnson and R. Silsbee, Coupling of electronic charge and spin at a ferromagnetic-paramagnetic metal interface, Phys. Rev. B **37,** 5312 (1988).